International Journal of Multiphase Flow 35 (2009) 987–1000

Contents lists available at ScienceDirect

International Journal of Multiphase Flow

journal homepage: www.elsevier.com/locate/ijmulflow

Flow boiling heat transfer characteristics of R123 and R134a in a micro-channel

Sehwan In *, Sangkwon Jeong

Cryogenic Engineering Laboratory, School of Mechanical, Aerospace and Systems Engineering, Korea Advanced Institute of Science and Technology, Guseong-dong, Yuseong-gu, Daejeon 305-701, Republic of Korea

ARTICLE INFO

Article history:
Received 3 December 2008
Received in revised form 3 July 2009
Accepted 9 July 2009
Available online 19 July 2009

Keywords:
Flow boiling heat transfer
Micro-channels
Wall superheat requirement

ABSTRACT

Flow boiling heat transfer in a single circular micro-channel of 0.19 mm ID has been experimentally investigated with R123 and R134a for various experimental conditions: heat fluxes (10, 15, 20 kW/m^2), mass velocities (314, 392, 470 kg/m^2 s), vapor qualities (0.2–0.85) and different saturation pressures (158, 208 kPa for R123; 900, 1100 kPa for R134a). The heat transfer trends between R123 and R134a are clearly distinguished. Whether nucleate boiling is suppressed at low vapor quality or not determines the heat transfer trend and mechanism in the flow boiling of micro-channels. High convective heat transfer coefficients in the two-phase flow of micro-channels enables nucleate boiling to be suppressed even at low vapor quality, depending on the wall superheat requirement for nucleate boiling. In the case of early suppression of nucleate boiling, specifically R123, heat transfer is dominated by evaporation of thin liquid films around elongated bubbles. In the contrary case, namely R134a, nucleate boiling is dominant heat transfer mechanism until its suppression at high vapor quality and then two-phase forced convection heat transfer becomes dominant. It is similar to the heat transfer characteristic of macro-channels except the enhancement of nucleate boiling and the short forced convection region.

1. Introduction

Micro-channels have their intrinsic advantages in heat exchanger application. They have larger contact area with fluid per unit volume and withstand higher pressure than macro-channels. The heat transfer coefficient inside them is, moreover, much higher at similar operating condition than that of macro-channels. An evaporative compact heat exchanger with micro-channels has been applied to many fields which need large heat transfer in limited space. It is used in a micro heat pump for microprocessor cooling or a portable cooling device (Munkejord et al., 2002), small scale stationary auxiliary power units (APU) based upon fuel cell technology (Kolb et al., 2007), a CO_2 transcritical system (Yun et al., 2005), and a cryosurgical probe for ablating tumors or treating heart arrhythmia (Marquardt et al., 1998).

Many researches have been done on the topic of flow boiling heat transfer in a micro-channel which is essential to design such an evaporative compact heat exchanger. Bao et al. (2000) measured local flow boiling heat transfer coefficients for R11 and R123 in a smooth copper tube with an inner diameter of 1.95 mm. Their experimental conditions were heat fluxes from 5 to 200 kW/m^2, mass velocities from 50 to 1800 kg/m^2 s, vapor qualities from 0 to 0.9 and system pressures from 200 to 500 kPa. They observed that heat transfer coefficients were strong functions of heat flux and system pressure but had very small mass velocity and vapor quality effects. They concluded that nucleate boiling was the dominant heat transfer mechanism in a micro-channel. Owhaib et al. (2004) investigated flow boiling heat transfer of R134a in vertical tubes with inner diameters of 1.7, 1.224 and 0.826 mm. They measured heat transfer coefficients for the heat flux range of 3–34 kW/m^2, the mass velocity range of 50–400 kg/m^2 s, vapor qualities up to 0.6 and two different system pressures of 645.8 and 862.6 kPa. It was found that heat transfer coefficients were highly dependent on heat flux and system pressure but moderately independent on mass velocity and vapor quality. Additionally, the heat transfer coefficients increased with decreasing inner diameter. Similar to Bao et al. (2000), they suggested nucleate boiling as the main heat transfer mechanism. Yun et al. (2005) reported local flow boiling heat transfer coefficients for CO_2 in rectangular micro-channels with hydraulic diameters from 1.08 to 1.54 mm. The experiment was performed at heat fluxes from 10 to 20 kW/m^2, mass velocities from 200 to 400 kg/m^2 s and saturation temperatures of 0, 5 and 10 °C. Their results indicated significant effects of heat flux and saturation pressure on a heat transfer coefficient like previous studies. The decrease of hydraulic diameter also increased the heat transfer coefficient. Many experimental studies together with Bao et al. (2000), Owhaib et al. (2004) and Yun et al. (2005) have shown that flow boiling heat transfer coefficients in micro-channels are mainly dependent on heat flux and

* Corresponding author. Tel.: +82 42 350 3079.
E-mail addresses: insh@kaist.ac.kr (S. In), skjeong@kaist.ac.kr (S. Jeong).

0301-9322/$ - see front matter © 2009 Elsevier Ltd. All rights reserved.
doi:10.1016/j.ijmultiphaseflow.2009.07.003

saturation pressure with small effect of mass velocity and vapor quality and suggested the nucleate boiling as a dominant heat transfer mechanism in micro-channel (Ribatski et al., 2006). Several studies such as Yan and Lin (1998) and Ohta et al. (2006), however, reported the existence of a two-phase forced convection region at high vapor quality where the heat transfer coefficient increased in proportion to mass velocity and had no effect of heat flux. Despite of many experimental studies, the heat transfer trends among them showed a little or large difference depending on the experimental conditions and the reason has not been clearly explained yet (Ribatski et al., 2006). It prevents us from finding out a general correlation for the flow boiling heat transfer coefficient in micro-channels. Further experimental researches are still necessary to understand the physical phenomena of various heat transfer trends.

Another important problem about flow boiling heat transfer in micro-channels is how small a channel can be classified as a micro-channel where the characteristics of heat transfer, two-phase flow patterns and pressure drops start to deviate from those of conventional channels. The macro-to-micro channel threshold diameter tells us the lower limit where the prediction methods of macro-channels for heat transfer coefficients, two-phase flow patterns and pressure drops can be applied with reliability. Moreover, the criterion helps to select correct micro-channel data among numerous experimental data for the analysis of micro-channel flow boiling. It reduces the confusion resulting from the mixed data of micro-channels and macro-channels in the analysis. Kew and Cornwell (1997) introduced a confinement number, Co and suggested the threshold criterion with limited data as

$$\mathrm{Co} = \left[\frac{\sigma}{g(\rho_L - \rho_V)D_h^2}\right]^{1/2} > 0.5 \quad (1)$$

where σ is surface tension, g is the gravitational acceleration, D_h is the hydraulic diameter of a flow channel and ρ_L and ρ_V are fluid densities of liquid and vapor phases, respectively. Jacobi and Thome (2002) proposed the conceptual criterion that bubble growth is confined by the channel wall, i.e. the channel diameter is similar to the bubble departure diameter. They, however, didn't present any practical correlation. In spite of several attempts, the reliable correlation for the threshold criterion has not been established yet due to lack of reliable experimental data to deduce the criterion and different trends among experimental data. Further experimental studies for the threshold criterion are also required together with those on heat transfer characteristics.

This paper describes an experimental investigation on the flow boiling heat transfer of R123 and R134a in a single circular micro-channel with the inner diameter of 0.19 mm. The test fluids of R123 and R134a have considerable differences of properties at ambient saturation temperature, such as saturation pressure, surface tension and liquid viscosity. Surface tension and liquid viscosity of R123 are nearly twice as large as those of R134a at ambient saturation temperature. Those properties have a direct influence on the fluid dynamic behavior of liquid and vapor flows in the flow boiling of micro-channels. Furthermore, saturation pressure and surface tension are important properties determining the wall superheat requirement for nucleate boiling. The change of heat transfer trends according to test fluid is investigated for various experimental conditions: heat fluxes (10, 15, 20 kW/m^2), mass velocities (314, 392, 470 kg/m^2 s), vapor qualities (0.2–0.85) and different saturation pressures. The heat transfer mechanism for each heat transfer trend, main parameters responsible for the variation of trends and its physical significance in the flow boiling heat transfer of micro-channels are also discussed.

2. Experimental apparatus and test conditions

2.1. Determination of channel diameter

It is very important to determine test channel diameter to use the data obtained from the experiment as fundamental data for the analysis of flow boiling heat transfer characteristics and mechanisms in micro-channels. The inner diameter of the test channel, therefore, was determined to satisfy the micro-channel criterion in consideration of the macro-to-micro channel threshold diameters which were suggested by several typical previous studies. The threshold diameters proposed by Kew and Cornwell (1997), Kandlikar and Grande (2003) and Jacobi and Thome (2002) were used for the purpose. Table 1 shows the threshold diameters which correspond to present experimental conditions. Kandlikar and Grande (2003) classified the range from 10 to 200 μm as micro-channels for two-phase flow applications; it was extended from the channel classification for gas flow. The threshold diameters suggested by Kew and Cornwell (1997) and Jacobi and Thome (2002) are already presented in the introduction section of this paper. The correlations for the bubble departure diameter in nucleate pool boiling, namely Kutateladze and Gogonin (1979), Jensen and Memmel (1986) and Borishanskiy et al. (1981), were used for the conceptual threshold diameter which Jacobi and Thome (2002) proposed. Dupont and Thome (2004) suggested that the bubble departure diameter in nucleate pool boiling can be considered as the approximation of the conceptual threshold diameter of Jacobi and Thome (2002). The correlations for the bubble departure diameter in nucleate pool boiling are summarized in Appendix A. The present channel diameter (0.19 mm) satisfies most of the micro-channel criterions as shown in Table 1.

2.2. Experimental setup and conditions

Fig. 1 shows the schematic diagram of an experimental apparatus. The experimental apparatus consisted of a closed loop: the reservoir, the subcooler, the magnetic gear pump, the sintered metal filter, the Coriolis mass flow controller, the temperature-adjusted entrance, the preheater, the test section and the condenser. Test fluid flowed along this closed loop in the direction of arrow. The reservoir had two thermoelectric modules attached on its opposite sides. The system pressure was controlled by adjusting the temperature of test fluid in the reservoir with thermoelectric modules because the test fluid was at a saturation state. The subcooler with a thermoelectric module made test fluid fully subcooled to prevent cavitation at the magnetic gear pump. Some of the test fluid pushed by the magnetic gear pump came back to the reservoir through a bypass line and the rest flowed into the test section. The mass flow rate of the test fluid passing the test section was controlled and simultaneously measured by the Coriolis mass flow controller (Brooks Instrument, QMBC2L). The test fluid past the mass flow controller became a moderately subcooled state by the temperature-adjusted entrance with a thermoelectric module and flowed into the preheater. The preheater controlled the vapor

Table 1
Macro-to-micro channel threshold diameter for present experimental conditions (unit: mm).

Refrigerant	Kew and Cornwell (1997)	Kandlikar and Grande (2003)	Kutateladze and Gogonin (1979)	Jensen and Memmel (1986)	Borishanskiy et al. (1981)
R123	1.905–1.961	0.2	0.243–0.267	0.272–0.295	0.417–0.473
R134a	1.475–1.561	0.2	0.185–0.196	0.208–0.220	0.211–0.232

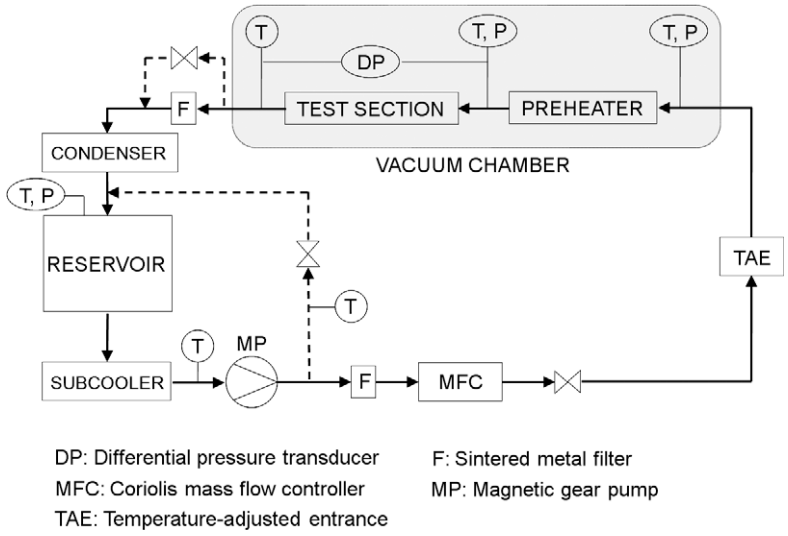

Fig. 1. Experimental apparatus.

quality of the test fluid which went into the test section. The test fluid returned to the reservoir past the condenser after heat transfer coefficients were measured in the test section.

The preheater and the test section were thermally insulated by a vacuum chamber. A great deal of attention was paid to the heat loss minimization because the mass flow rate was so small that the measured results were very sensitive to heat loss. Multilayer insulation was applied around the preheater and the test section to reduce heat loss by radiation. Band and plate heaters were also installed on the top flange and the side wall of the vacuum chamber to make its temperature similar to that of experimental conditions and reduce heat loss by free molecular conduction and radiation. The heat loss in the test section was measured by a preliminary heating experiment. While the inside of the test section was maintained at a vacuum, the heat was applied to the test section in the experiment. The total heat applied to the test section, is transferred to the outside because the inside of the test section is in a vacuum and no fluid flow taking the heat exists. The heat applied to the test section, therefore, can be considered as the heat going outside, namely heat loss in the test section. The temperature differences between the outer wall of the micro-channel and the outside of the vacuum chamber were measured according to the amount of heat applied to the test section. The correlation of heat loss was obtained as the function of the temperature difference between the outer wall of the micro-channel and the outside of the vacuum chamber. The heat loss in the flow boiling experiment was estimated approximately within 11.8 mW, 4.7–9.5% of heat input. Details of the test section are shown in Fig. 2. The inner and outer diameters of the micro-channel were 0.19 and 1.59 mm, respectively. It was made of stainless steel (Stainless steel 316) and the length was 31 mm. Both ends of the micro-channel were connected with thin stainless steel tubes with the thickness of 0.3 mm, the length of 35 mm and the outer diameter of 1.59 mm to reduce heat loss by conduction. The heat input was applied to the test section by the indirect heating method that uses the Joule heating of the nichrome wire (OD: 0.2 mm) wound around the outside wall as shown in Fig. 2. Thermally conductive silicon adhesive (Dow Corning, SE4485) was filled for better

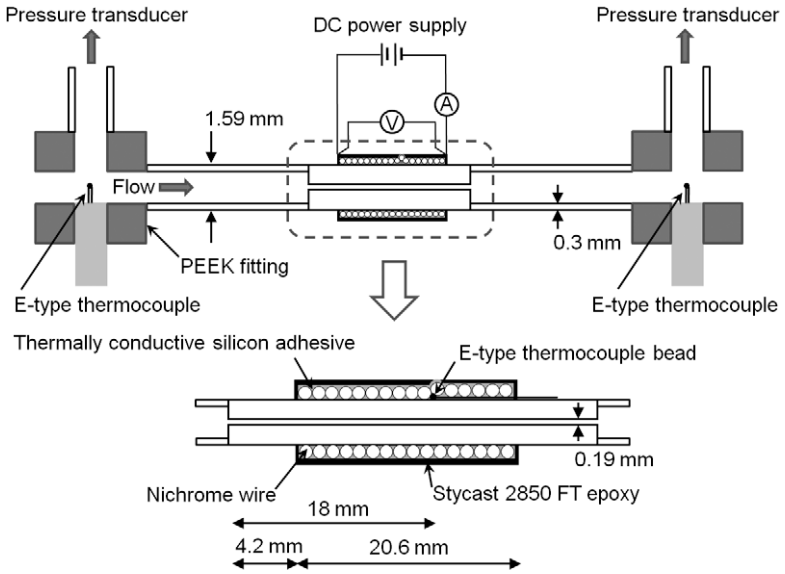

Fig. 2. Test section.

Table 2
Error of sensors and measuring instruments.

Sensor or measuring instrument	Error
Coriolis mass flow controller	$\pm 1.4 \times 10^{-7}$ kg/s
Absolute pressure transducer	±0.3 kPa (for R123), ±3.4 kPa (for R134a)
Differential pressure transducer	±0.9 kPa
E-type thermocouple	±0.1 K
Voltmeter (Keithley 175A)	±3 mV
Ammeter (Fluke 187)	±0.4 mA

Table 3
Experimental conditions.

Parameter	Condition
Heat flux	10, 15, 20 kW/m^2
Mass velocity	314, 392, 470 kg/m^2 s
Vapor quality	0.2–0.85
Saturation pressure (saturation temperature)	R123: 158 kPa (40.7 °C), 208 kPa (49.3 °C) R134a: 900 kPa (35.5 °C), 1100 kPa (43.0 °C)

thermal contact between the outer wall of the channel and the nichrome wire, which were fixed by Stycast 2850FT epoxy. The indirect heating method was also applied to the preheater where the nichrome wire was wound around the stainless steel tube 1.59 mm in outer diameter, 0.3 mm in thickness and 43 mm in length. The currents applied to the nichrome wires of the preheater and the test section were provided by the precision DC power supply (FinePower, FD-1508D). A single E-type thermocouple with the outer diameter of 0.127 mm was soldered on the outer surface of the micro-channel for the measurement of channel surface temperature. Three E-type thermocouples with the outer diameter of 0.025 mm were inserted into the preheater inlet, the test section inlet and the test section outlet for the measurement of test fluid temperatures, respectively. The cold junctions of thermocouples were maintained at 0 °C by an ice point calibration reference chamber (OMEGA, TRCIII). The pressures of test fluid were also measured at the same places with inserted thermocouples by two absolute pressure transducers (Sensotec, FPA-1-KH for R123, FPA-1-CR for R134a) and one differential pressure transducer (Validyne, DP10-42). The thermocouples used in the experiment had been calibrated for the temperature range of experimental conditions with ASTM certified glass thermometers (OMEGA; ASTM-63C, 64C, 65C, 66C). In addition, the calibration of the pressure transducers had been carried out for the pressure range of experimental conditions with the internal pressure modules of a MC5 multifunction calibrator (Beamex; Module INT60, Module INT1C). Voltage drops and currents in the nichrome wires wound around the preheater and the test section were measured by digital multimeters (Keithley 175A for voltage drop, Fluke 187 for current). The accuracy of sensors and measuring instruments which makers guarantee and the standard estimation errors of thermocouples and pressure transducers after calibration are shown in Table 2. The experiment was performed for each test fluid (R123, R134a) with the variation of four parameters: heat flux, mass velocity, vapor quality and saturation pressure. The experimental conditions are summarized in Table 3.

3. Data reduction

The local flow boiling heat transfer coefficient, h, is defined as the heat flux into test fluid divided by wall superheat.

$$h = \frac{q''}{T_{wi} - T_{SAT}} \tag{2}$$

where q'' is the heat flux into test fluid, T_{wi} is the inner wall temperature of the micro-channel and T_{SAT} is the saturation temperature of test fluid. The heat flux is calculated by dividing the rate of heat generation in the test section by the heated inner surface area of the micro-channel. The rate of heat generation is determined by the product of voltage drop, V_t, and current, I_t, measured at the nichrome wire wound around the test section.

$$q'' = \frac{I_t \cdot V_t}{\pi \cdot D_i \cdot L_h} \tag{3}$$

where D_i and L_h are the inner diameter and the heating length of the micro-channel, respectively. The inner wall temperature is calculated from the measured outer wall temperature using a one-dimensional heat conduction equation as

$$T_{wi} = T_{wo} - \dot{q}_t \cdot \frac{\ln(D_o/D_i)}{2 \cdot \pi \cdot L_h \cdot k_c} \tag{4}$$

where T_{wo} is the outer wall temperature of the micro-channel, $\dot{q}_t$ is the rate of heat generation in the test section and, D_o and k_c are the outer diameter and the thermal conductivity of the micro-channel, respectively. The saturation temperature of test fluid is determined by its saturation pressure calculated from the inlet pressure and the pressure drop measured in the test section. The followings are details for the calculation of the saturation pressure. As shown in Fig. 2, the test section has a sudden contraction and a sudden enlargement at the inlet and the outlet of the micro-channel with a sharp edge respectively. The pressure drop measured in the test section, therefore, includes the pressure drop by the sudden contraction at the micro-channel inlet and the pressure recovery by the sudden enlargement at the micro-channel outlet as well as the pressure drop in the micro-channel; the pressure drop in the thin stainless steel tubes connected with both ends of the micro-channel is negligible. The micro-channel inlet pressure (pressure just downstream of the sudden contraction) and the micro-channel outlet pressure (pressure just upstream of the sudden enlargement) are calculated from the inlet pressure and the pressure drop measured in the test section using pressure correlations for a sudden contraction and a sudden enlargement. Finally, the local saturation pressure is determined from the micro-channel inlet pressure and the micro-channel outlet pressure with the assumption that the pressure drop in the micro-channel is linear. The pressure drop and the pressure recovery at the sudden contraction and the sudden enlargement are determined by the pressure correlations which Collier and Thome (1994) suggested, respectively. The pressure drop at the sudden contraction is calculated as

$$\Delta P_C = \frac{G^2}{2 \cdot \rho_L}\left[\left(\frac{1}{C_C} - 1\right)^2 + \left(1 - R_A^2\right)\right] \cdot \left[1 + \left(\frac{\rho_L}{\rho_V} - 1\right) \cdot x\right] \tag{5}$$

where G is mass velocity in the micro-channel, ρ_L and ρ_V are liquid density and vapor density, respectively, x is vapor quality and R_A is a cross sectional area ratio, a small cross sectional area divided by a large cross sectional area. The contraction coefficient, C_C is determined from the following equation proposed by Chisholm (1983).

$$C_C = \frac{1}{0.639 \cdot (1 - R_A)^{0.5} + 1} \tag{6}$$

The pressure recovery at the sudden enlargement is calculated as

$$\Delta P_E = \frac{G^2}{\rho_L} \cdot R_A \cdot (1 - R_A) \cdot \left[1 + \left(\frac{\rho_L}{\rho_V} - 1\right) \cdot x\right] \tag{7}$$

Though the pressure drop and the pressure recovery at the sudden contraction and the sudden enlargement were considered for calculation of the saturation pressure, the pressure changes by the sudden contraction and the sudden enlargement were very small compared with the pressure drop in the micro-channel.

The vapor quality is determined on a thermodynamic basis with saturation pressure and specific enthalpy at the measuring point. The specific enthalpy is calculated from an energy balance equation as follows.

$$i_{mp} = i_{pre} + \frac{\dot{q}_{pre}}{\dot{m}} + \frac{\dot{q}_t}{\dot{m}} \cdot \frac{x_h}{L_h} \quad (8)$$

where i_{mp} is specific enthalpy at the measuring point, i_{pre} is specific enthalpy at the preheater inlet determined by the temperature and the pressure measured at that point, $\dot{q}_{pre}$ is the rate of heat generation by the Joule heating of the nichrome wire in the preheater, $\dot{m}$ is the mass flow rate of test fluid and x_h is the distance from the upstream end of the heating region to the measuring point in the test section.

All the thermodynamic, transport and physical properties of R123 and R134a, including density, enthalpy, viscosity, thermal conductivity, and so on, were obtained from software REFPROP version 8.0 developed by the National Institute of Standards and Technology (NIST). The propagation of the measurement uncertainties through data reduction was estimated by software EES (F-chart software, version 7.952). Based on the calculation method suggested by Taylor and Kuyatt (1994), the EES software estimates the uncertainty of the resultant variable through data reduction from the uncertainties of measured variables. The measurement uncertainties in the present experiment are shown in Table 2. Furthermore, the uncertainty of heat input was considered in the calculation of uncertainty propagation. From the preliminary heating experiment, the heat loss in the flow boiling experiment was estimated within 11.8 mW, 4.7–9.5% of heat input as mentioned in the Section 2.2. The maximum uncertainty of heat transfer coefficients in the flow boiling heat transfer was estimated at ±13.8% from the analysis of uncertainty propagation.

4. Experimental results and discussion

4.1. Single phase heat transfer

The validity of the present experimental apparatus was examined by the experiment with subcooled R123 in single phase heat transfer. Single phase heat transfer coefficients were measured at mass velocities of 392 and 470 kg/m^2 s with two different heat fluxes of 7 and 9 kW/m^2. The mass velocity conditions are the same as those given in the flow boiling experiment except the mass velocity condition of 314 kg/m^2 s. The heat loss was considered in data reduction for heat transfer coefficients because the error by heat loss was large compared with flow boiling heat transfer. The heat transfer coefficient in single phase heat transfer is much smaller than that in flow boiling heat transfer and the fluid temperature in single phase heat transfer increases according to applied heat flux contrary to flow boiling heat transfer. It leads to high test section surface temperature and large heat loss compared with flow boiling heat transfer. Fig. 3 shows the comparison of experimental data with theoretical values where Nu_D and Gz_D represent Nusselt number and Graetz number based on the inner diameter of the micro-channel, respectively. The theoretical values are for laminar flow in a uniform heat flux condition and given by Kays and Crawford (1993). The experimental data shows a good agreement with the theoretical values.

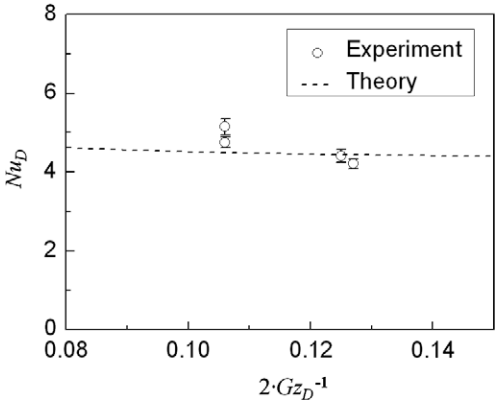

Fig. 3. Comparison of experimental data with theoretical values in single phase heat transfer.

4.2. Flow boiling heat transfer characteristics

4.2.1. Heat transfer characteristics in flow boiling of R123

Fig. 4 shows the effect of mass velocity on the flow boiling heat transfer of R123, which is plotted along the vapor quality at different heat fluxes and saturation pressures. The strong effect of mass velocity is found at low saturation pressure, while insignificant at high saturation pressure. At low vapor quality, the heat transfer coefficient generally increases according to the increase in mass velocity, which is remarkable at the high heat flux condition of low saturation pressure as shown in Fig. 4(a). The increase in mass velocity, however, results in the deterioration of heat transfer at high vapor quality, which results from the intermittent dry-out of the liquid film surrounding elongated bubbles. Its detail will be discussed in the next section of the heat transfer mechanism.

The effect of heat flux on flow boiling heat transfer at several mass velocities and saturation pressures is shown in Fig. 5. The heat transfer coefficient is increased by heat flux. The effect is more significant at high vapor quality than at low vapor quality. The heat

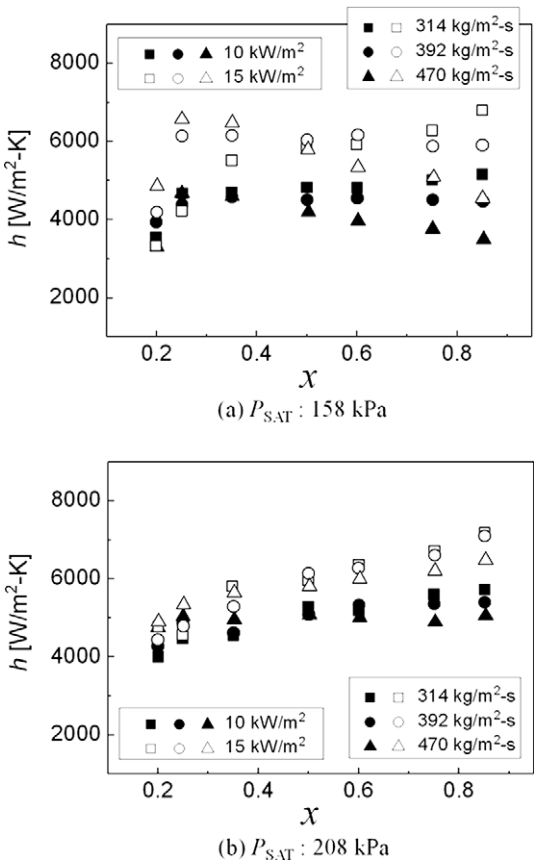

Fig. 4. Effect of mass velocity on flow boiling heat transfer coefficients of R123 with respect to vapor quality at different heat fluxes and saturation pressures.

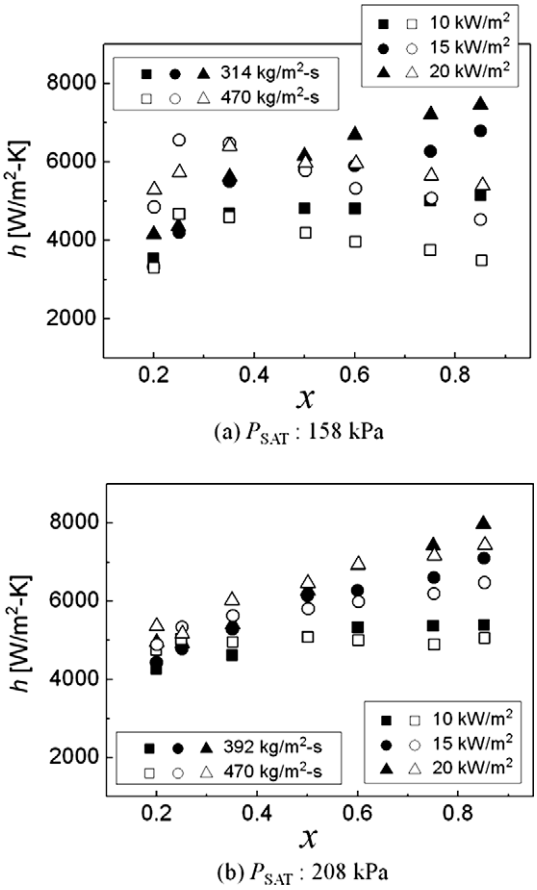

Fig. 5. Effect of heat flux on flow boiling heat transfer coefficients of R123 with respect to vapor quality at different mass velocities and saturation pressures.

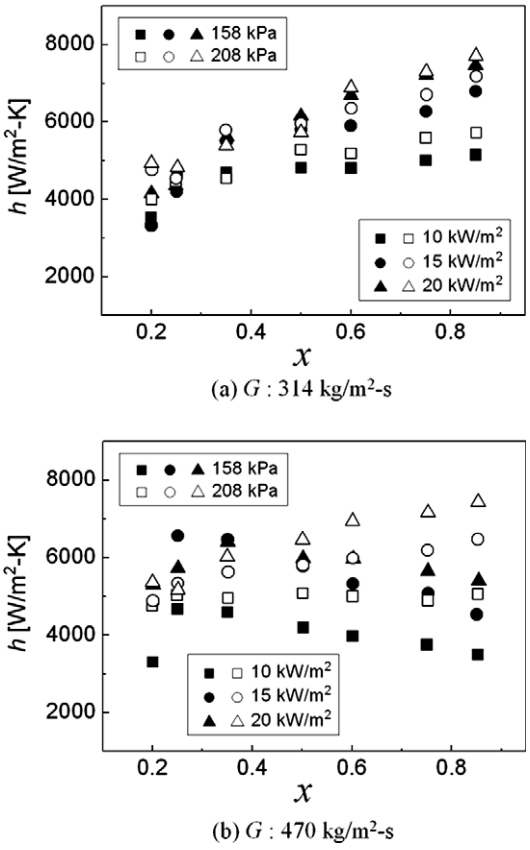

Fig. 6. Effect of saturation pressure on flow boiling heat transfer coefficients of R123 with respect to vapor quality at different mass velocities and heat fluxes.

transfer trend with regard to vapor quality, however, changes at the high mass velocity condition of low saturation pressure and the deterioration of heat transfer coefficients by heat flux also occurs. The change of the heat transfer trend and the deterioration of heat transfer coefficients result from the intermittent dry-out which is promoted by high mass velocity as mentioned in the above paragraph.

The saturation pressure effect is examined through the rearrangement of experimental data as shown in Fig. 6. The change of heat transfer coefficients by saturation pressure depends on experimental conditions: mass velocity and heat flux. The change is significant at the high mass velocity condition, while small at the low mass velocity condition.

4.2.2. Heat transfer characteristics in flow boiling of R134a

The heat transfer characteristics of R134a are substantially different from those of R123. Fig. 7 shows the effect of mass velocity on the flow boiling heat transfer coefficient of R134a at different heat fluxes. The mass velocity effect is small except high vapor quality where the relatively large increase in heat transfer coefficients by mass velocity rise is observed. The heat transfer coefficients, moreover, have almost constant values at low and intermediate vapor quality which means the insignificant vapor quality effect.

Fig. 8 indicates the effect of heat flux on flow boiling heat transfer at different mass velocities. The definite increase in heat transfer coefficients is found by heat flux rise at low vapor quality. The heat flux effect, however, becomes smaller and smaller as vapor quality increases, and finally disappears at high vapor quality. In addition, the decline of the heat flux effect becomes more obvious

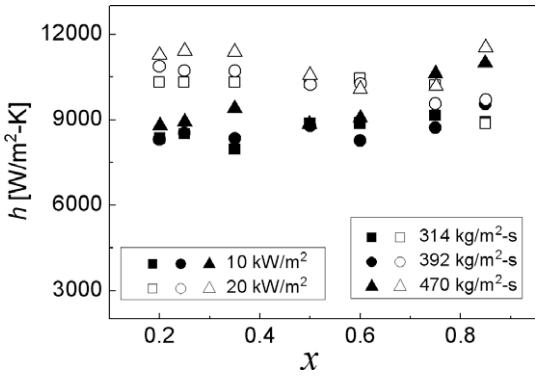

Fig. 7. Effect of mass velocity on flow boiling heat transfer coefficients of R134a with respect to vapor quality at different heat fluxes of saturation pressure, 1100 kPa.

at high mass velocity. It resembles the suppression of nucleate boiling at high vapor quality of macro-channels; the suppression effect also gets larger at high mass velocity.

The saturation pressure effect at different mass velocities is shown in Fig. 9. The heat transfer coefficients increase with the increase in saturation pressure. Like the heat flux effect, the saturation pressure effect becomes smaller and smaller as vapor quality increases, and insignificant at high vapor quality. It is also similar to the feature resulting from the suppression of nucleate boiling at high vapor quality of macro-channels.

The boiling heat transfer coefficients of R134a indicate insignificant mass velocity and vapor quality effects but strong depen-

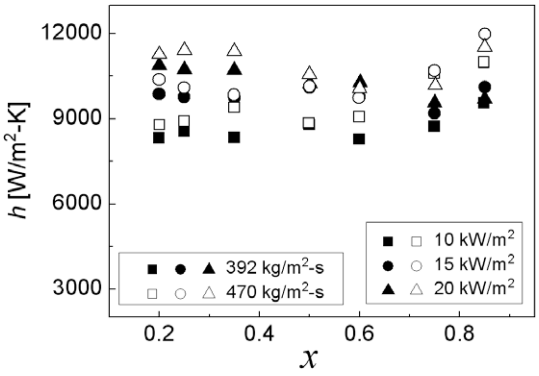

Fig. 8. Effect of heat flux on flow boiling heat transfer coefficients of R134a with respect to vapor quality at different mass velocities of saturation pressure, 1100 kPa.

dence on heat flux and saturation pressure at low and intermediate vapor quality. The heat transfer characteristics are similar to those of a nucleate boiling region in macro-channels. The features of two-phase forced convection, on the other hand, appear at high vapor quality with large effects of mass velocity and vapor quality.

4.3. Flow boiling heat transfer mechanism

4.3.1. Heat transfer mechanism for the flow boiling of R123

The flow pattern of two-phase flow is closely related with the flow boiling heat transfer in micro-channels as it is so in macro-channels. Especially, the flow pattern has a critical effect on the flow boiling heat transfer of R123 in micro-channels. The details about it will be given at next paragraphs. Many flow pattern maps for micro-channels have been reported in the literature, but they were tentative (Thome, 2004) and had a disagreement on flow pattern transition boundaries among them (Kawahara et al., 2002). It, therefore, is still difficult to predict the flow pattern in the flow boiling of micro-channels with reliability. Nevertheless, it is recognizable what flow pattern is predominant in micro-channels from the flow pattern observations reported in previous studies. Since no stratification of the liquid occurs in micro-channels due to the dominant surface tension force, the flow pattern observations in micro-channels indicate that the flow pattern is represented by the bubbly flow, the elongated bubble flow (intermittent flow), the annular flow and the flow with partial dry-out (Thome, 2004; Kandlikar, 2002). The bubbly flow only appears at subcooled boiling or very low vapor quality, and the flow with partial dry-out mainly exists at high vapor quality. The elongated bubble flow and the annular flow, therefore, are considered as the primary flow regimes in micro-channels. Lee and Mudawar (2005) observed the flow pattern in the rectangular channel of 231 × 713 μm during the flow boiling process of R134a. Their mass velocity range was 127–654 kg/m^2 s similar to that in the present experiment. They found that the transition from the slug flow (elongated bubble flow) to the annular flow occurred at higher vapor quality than in macro-channels where the transition mostly occurs at the vapor quality of 0.25–0.35. The transition was sometimes observed even beyond the vapor quality of 0.5 in their experiment. In addition, Kawahara et al. (2002) investigated the two-phase flow pattern in a 100 μm diameter circular tube with de-ionized water and nitrogen gas. The superficial velocity ranges of liquid and gas were j_L = 0.02–4 m/s and j_G = 0.1–60 m/s, respectively, in their experiment. The ranges include the superficial velocities of liquid and vapor applied to the present experiment. They observed that the alternate flows of the liquid slug and the gas core with a liquid film appeared with some time fraction according to their experimental conditions. The time fraction and the liquid film shape depended on the superficial velocities of liquid and gas. The authors classified the flow pattern into four flow regimes based on the time fraction and the liquid film shape: slug-ring flow, ring-slug flow, multiple flow and semi-annular flow. Although the authors defined the flow with very small time fraction of the liquid slug as a semi-annular flow, all flow regimes in their experiment can be considered as the elongated bubble flow in that the liquid slug exists between gas cores with a liquid film. The studies by Lee and Mudawar (2005) and Kawahara et al. (2002) suggest that the elongated bubble flow is the dominant flow regime in the two-phase flow of micro-channels. The flow boiling heat transfer characteristics of R123 in the present experiment are well described by the heat transfer model based on the elongated bubble flow regime. The behavior of the liquid film thickness surrounding elongated bubbles in the elongated bubble flow explains the effects of mass velocity, heat flux and saturation pressure on the heat transfer coefficient in the present experiment for R123. The details will be given at the following paragraphs.

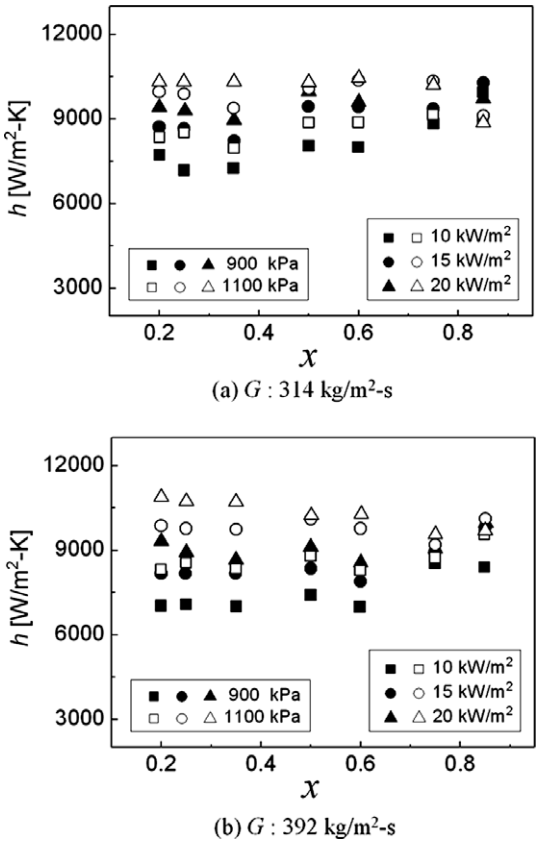

Fig. 9. Effect of saturation pressure on flow boiling heat transfer coefficients of R134a with respect to vapor quality at different mass velocities and heat fluxes.

The heat transfer characteristics of R123 mentioned in the Section 4.2.1 are clearly distinguished from those of macro-channels. The heat transfer coefficients of macro-channels are dependent on heat flux and saturation pressure at low vapor quality, but mass velocity and vapor quality at high vapor quality. The heat transfer features of R123 have a good qualitative agreement with the heat transfer model based on the evaporation heat transfer of thin liquid films around elongated bubbles successively passing the micro-channel, namely elongated bubble flow regime. The heat transfer model was suggested by Jacobi and Thome (2002) and developed into the sophisticated model applicable to the flow boiling in micro-channels by Thome et al. (2004). They made a theoretical description of the transient variation of a local heat transfer

coefficient in the elongated bubble flow, specifically the cyclic passage of a liquid slug, an elongated bubble and a vapor slug in case that the liquid film around the elongated bubble is completely evaporated. A time-averaged local heat transfer coefficient is obtained from the transient local heat transfer coefficients predicted by the model during the period of the cycle. The model, however, includes three parameters which are difficult to predict theoretically, but have a strong effect on the heat transfer coefficient. They are the minimum thickness of the liquid film at dry-out (δ_{min}), the correction factor for the initial thickness of the liquid film (C_δ) and the pair frequency of the bubble (f). Dupont et al. (2004) empirically optimized the values of the parameters according to the experimental database taken from several independent studies concerning the flow boiling heat transfer in micro/mini-channels. The specific equations with respect to the heat transfer model and the optimized parameters will not be given here because they consist of a considerable number of equations which need the explanation for a basic understanding. For the detailed equations, the reader is recommended to refer to Thome et al. (2004) and Dupont et al. (2004). Though the use of the empirical parameter values in the model led to good predictions of heat transfer coefficients for their experimental database, the general application of the heat transfer model using the empirical parameter values seems to be difficult because the parameters are determined only from the limited experimental database without the physical base. In this section, we, therefore, focus on how the heat transfer model can qualitatively describe our experimental results rather than the direct comparison with the heat transfer model using the empirical parameter values. Thome et al. (2004), in addition, used a homogeneous model to calculate void fraction and two-phase velocity at the desired vapor quality due to the absence of a reliable void fraction model. The homogeneous model may be acceptable because it made relatively good predictions of frictional pressure drop in the two-phase flow of micro-channels according to Ribatski et al. (2006). Ribatski et al. (2006) compared the extensive experimental database for two-phase frictional pressure drop in mini/micro-channels with various existing prediction methods including the homogeneous model. The discussion on the heat transfer mechanism of R123 in this section is also based on the homogeneous model. The homogeneous model assumes that the velocities of vapor phase and liquid phase are same. The equation for void fraction is derived from the assumption as the function of vapor quality (x), liquid density (ρ_L) and vapor density (ρ_V). Void fraction (α) is expressed as

$$\alpha = \frac{A_V}{A} = \frac{\rho_L \cdot \rho_V}{(1-x)\cdot\rho_V + x\cdot\rho_L}\cdot\frac{x}{\rho_V} = \frac{\rho}{\rho_V}\cdot x \tag{9}$$

where A and A_V are the cross sectional areas of the channel and occupied by vapor phase, respectively, and ρ is average density of two-phase fluid defined as

$$\frac{1}{\rho} = \frac{1-x}{\rho_L} + \frac{x}{\rho_V} \tag{10}$$

The key parameter to determine heat transfer coefficients in this heat transfer model is the liquid film thickness surrounding elongated bubbles because the heat transfer in the vapor or liquid slugs following the bubbles is very small. The heat transfer coefficients are in inversely proportion to film thickness. Liquid film thickness depends on mass velocity, heat flux, saturation pressure and vapor quality. The three following paragraphs will explain how liquid film thickness in the elongated bubble flow changes with respect to mass velocity, heat flux, saturation pressure and vapor quality, what effect the change of liquid film thickness has on heat transfer coefficients and how well it describes our experimental results. The explanations will be given in the order of the effects of mass velocity and vapor quality, the heat flux effect and the saturation pressure effect on the heat transfer coefficient.

From fluid dynamics of the elongated bubble flow without phase change by heat transfer, liquid film thickness at high bubble velocity is determined by viscous boundary layer thickness (Aussillous and Quéré, 2000). Its order of magnitude was presented by Moriyama and Inoue (1996) and Thome et al. (2004) as follows.

$$\frac{\delta}{D} \sim \left(\frac{\nu_L}{U_b}\cdot D\right)^{0.42} \quad \text{for } \frac{\rho_L\cdot D}{\sigma}\cdot U_b^2 > 2 \tag{11}$$

where δ and D are liquid film thickness and the channel diameter respectively, ν_L is the kinematic viscosity of liquid, U_b is bubble velocity, ρ_L is liquid density and σ is surface tension. In homogenous flow, bubble velocity is calculated from Eq. (9) as

$$U_b = \frac{G\cdot x}{\rho_V\cdot\alpha} = G\cdot\left(\frac{x}{\rho_V} + \frac{1-x}{\rho_L}\right) \tag{12}$$

where G is mass velocity. The present experimental conditions satisfy the criterion of Eq. (11). ($\rho_L \cdot D \cdot U_b^2/\sigma > 549$ in the present experiment) Eqs. (11) and (12) indicate that the increase in mass velocity or vapor quality leads to the decrease in liquid film thickness. The heat transfer coefficient, therefore, increases with the increase in mass velocity or vapor quality. Excess decrease in liquid film thickness by mass velocity or vapor quality, however, gives rise to its intermittent dry-out in flow boiling heat transfer where a portion of the liquid film is completely evaporated by heat flux. Once the intermittent dry-out occurs, the increase in mass velocity or vapor quality decreases the heat transfer coefficient because the intermittent dry-out region is expanded by heat flux according to the decrease in liquid film thickness. It explains that the heat transfer coefficient decreases with the increase in mass velocity or vapor quality at high vapor quality or high mass velocity where film thickness is very thin as shown in Fig. 4. The change of liquid film thickness by mass velocity or vapor quality in the elongated bubble flow well describes the effects of mass velocity and vapor quality observed in the experiment.

Liquid film thickness in flow boiling heat transfer is also affected by heat flux because the evaporation by heat transfer occurs at the liquid film. As the rear of the elongated bubble is approached, film thickness decreases more and more from its initial thickness formed at the front meniscus of the bubble due to the evaporation by heat flux. The initial thickness of the liquid film is determined by Eq. (11). The relation between liquid film thickness and heat flux is examined in detail with the analytic expression for the decrement of liquid film thickness at the rear end of the elongated bubble. With the assumption that liquid film thickness is very thin compared with the inner radius of the channel and intermittent dry-out of the film does not occur, the decrement of liquid film thickness is expressed as

$$\Delta\delta = \frac{q''}{\rho_L\cdot i_{fg}} t_b \tag{13}$$

where q'' is heat flux, i_{fg} is the enthalpy of vaporization and t_b is the bubble passing time which means the time it takes for an elongated bubble to pass the position. Bubble passing time in Eq. (13) is determined as follows. When the main heat transfer mechanism is not nucleate boiling but evaporation of thin liquid films around elongated bubbles, the additional nucleation of bubbles does not occur during a flow boiling process except for low vapor quality near zero where elongated bubbles are formed. The bubble departure frequency at the low vapor quality, therefore, determines the period of pairs (liquid slug and elongated bubble) or triplets (liquid slug, elongated bubble and vapor slug, namely intermittent dry-out) which pass the channel successively. When intermittent dry-out

does not take place, bubble passing time is consequently calculated for homogeneous flow as follows.

$$t_b = \tau \cdot \frac{\rho}{\rho_V} \cdot x = \frac{\rho}{\rho_V \cdot f} \cdot x \tag{14}$$

where τ is the period of pairs, ρ is the average density of two-phase fluid and f is the bubble departure frequency at the low vapor quality. With regard to the bubble departure frequency, the general correlation in the flow boiling of micro-channels does not exist yet. Lie and Lin (2005) performed some experiment about the saturated flow boiling heat transfer of R134a in a horizontal narrow annular duct with the gap of 1 and 2 mm, and suggested the empirical correlations for the bubble departure diameter and its frequency. Their correlations are used as alternatives in this paper. The correlations are as follows.

$$\frac{d_p}{\sqrt{\sigma/\{g \cdot (\rho_L - \rho_V)\}}} = 0.353 \cdot \left(\frac{\rho_L}{\rho_V}\right)^{0.5} \mathrm{Re}_L^{-0.2} \cdot \mathrm{Bo}^{0.2} \cdot \mathrm{Co}^{0.19} \tag{15}$$

$$\frac{f \cdot d_p}{\mu_L/(\rho_L \cdot D_h)} = 3.7 \cdot \mathrm{Re}_L^{1.33} \cdot \mathrm{Pr}_L^2 \cdot \mathrm{Bo}^{0.725} \cdot \mathrm{Co}^{0.59} \tag{16}$$

where d_p and f are the bubble departure diameter and its frequency respectively, σ is surface tension, g is the gravitational acceleration, μ_L is the viscosity of liquid and D_h is the hydraulic diameter. Re_L, Pr_L, Bo and Co represent the Reynolds number of liquid flow, the Prandtl number of liquid, the Boiling number and the Confinement number defined as

$$\mathrm{Re}_L = \frac{G \cdot D_h \cdot (1-x)}{\mu_L} \tag{17}$$

$$\mathrm{Pr}_L = \frac{c_{P,L} \cdot \mu_L}{k_L} \tag{18}$$

$$\mathrm{Bo} = \frac{q''}{G \cdot i_{fg}} \tag{19}$$

$$\mathrm{Co} = \left[\frac{\sigma}{g(\rho_L - \rho_V)D_h^2}\right]^{1/2} \tag{20}$$

where G is mass velocity, x is vapor quality, $c_{p,L}$ is the specific heat of liquid at constant pressure, k_L is the thermal conductivity of liquid, q'' is heat flux and i_{fg} is the enthalpy of vaporization. Eqs. (14) and (16) indicate that bubble passing time is in inverse proportion to heat flux. When heat flux increases, the bubble passing time term in Eq. (13), therefore, decreases. The change rate of bubble passing time, however, is less than the half of the heat flux change rate for present experimental conditions. The decrement of liquid film thickness at the rear end of the elongated bubble ($\Delta\delta$) in Eq. (13), therefore, gets larger when heat flux is increased. Consequently, average liquid film thickness becomes thinner and heat transfer coefficients are increased by heat flux rise. Furthermore, the heat flux effect gets larger at high vapor quality because the bubble passing time in Eq. (13) is proportional to vapor quality; the relation between bubble passing time and vapor quality is found in Eq. (14). The heat flux effects shown in Fig. 5 except for the high mass velocity case of Fig. 5(a), therefore, are well described by the behavior of liquid film thickness estimated from Eq. (13). On the other hand, the high mass velocity case of Fig. 5(a) shows the different heat transfer feature that the heat transfer coefficient sharply increases at low vapor quality and then decreases at intermediate and high vapor quality. The different heat transfer feature results from the intermittent dry-out mainly by high mass velocity mentioned in the previous paragraph. The intermittent dry-out can occur by heat flux as well as mass velocity and the deterioration of heat transfer coefficients by heat flux is found at low vapor quality of the high mass velocity case of Fig. 5(a). The experimental results for the effects of mass velocity and heat flux, however, indicate that the mass velocity is more critical to the intermittent dry-out at present experimental conditions.

Another factor affecting liquid film thickness is saturation pressure, which changes the physical properties of fluid and the bubble departure frequency. The density of saturated vapor is sensitive to the change of saturation pressure while that of saturated liquid is not; the density of saturated vapor increases as saturation pressure rises. The bubble velocity, therefore, is faster for identical mass velocity at low saturation pressure than at high saturation pressure and consequently has a larger increment for the identical increase in mass velocity because average density is smaller at low saturation pressure. It makes the effect of mass velocity on liquid film thickness larger at low saturation pressure. With regard to the bubble departure frequency, it is found from Eq. (16) that the bubble departure frequency decreases for identical conditions (mass velocity, heat flux and vapor quality) as the saturation pressure decreases. When the saturation pressure decreases, the bubble passing time, therefore, increases from Eq. (14) because the bubble departure frequency is proportional to the saturation pressure; the change of the density ratio (ρ/ρ_V) by pressure in Eq. (14) is negligible compared with that of the bubble departure frequency. The increase in bubble passing time by the reduced saturation pressure leads to the decrease in average liquid film thickness from Eq. (13); the change of the denominator ($\rho_L \cdot i_{fg}$) in Eq. (13) by pressure is very small compared with that of the bubble passing time (t_b). Liquid film thickness, therefore, gets thinner for identical heat flux at low saturation pressure and the effect of heat flux on liquid film thickness gets larger. As a consequence, the effects of mass velocity and heat flux on liquid film thickness around the elongated bubble become larger at low saturation pressure because the average density of fluid and the bubble departure frequency decrease in proportion to saturation pressure. It means that the effects of mass velocity and heat flux on heat transfer coefficients also become larger at low saturation pressure because heat transfer coefficients are determined by liquid film thickness. It explains why the effects of mass velocity and heat flux on heat transfer coefficients are much larger at low saturation pressure as shown in Fig. 4 and 5.

As discussed up to now, the heat transfer characteristics of R123 in present experimental conditions are well described by the behavior of liquid film thickness around elongated bubbles in the elongated bubble flow. It suggests that the flow boiling heat transfer of R123 in the present experimental conditions is dominated by the evaporation of the thin liquid film around the elongated bubble.

4.3.2. Heat transfer mechanism for the flow boiling of R134a

The experimental results of R134a show that the heat transfer characteristics are clearly different from those of R123 even for the same micro-channel size. Fig. 10 indicates the difference by

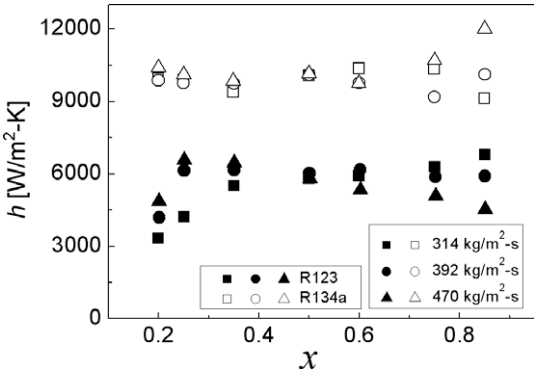

Fig. 10. Comparison of mass velocity effects in the flow boiling heat transfer of R123 and R134a (q'': 15 kW/m^2, P_{SAT}: 158 kPa for R123, P_{SAT}: 1100 kPa for R134a).

comparing mass velocity effects in the flow boiling heat transfer of R123 and R134a. As shown in Figs. 7–9, the flow boiling heat transfer of R134a have insignificant dependence on mass velocity and vapor quality while strong dependence on heat flux and saturation pressure at low and intermediate vapor quality, which are similar to the characteristics of nucleate boiling. The features of two-phase forced convection, on the other hand, appear at high vapor quality with the large effects of mass velocity and vapor quality. Nevertheless, it is necessary to check whether the heat transfer mechanism applied to the flow boiling heat transfer of R123, namely evaporative heat transfer of thin liquid films around elongated bubbles, also dominates that of R134a, because the experimental data of R123 sometimes show the heat transfer characteristics of R134a at a specific experimental condition. For example, the high mass velocity case of Fig. 5(a) indicates insignificant vapor quality and strong heat flux effects on heat transfer coefficients. Liquid film thickness between R123 and R134a for identical mass velocity and heat flux conditions is compared to check whether the heat transfer mechanism by the evaporation of a liquid film is applied to the flow boiling heat transfer of R134a in the present experiment. The initial liquid film thickness ratio and the liquid film thickness decrement ratio of R134a to R123 are calculated for the comparison. The ratio of the initial liquid film thickness formed at the front meniscus of an elongated bubble is determined by Eq. (11). The decrement of liquid film thickness by heat flux at the rear end of the elongated bubble is calculated from Eqs. (13) and (14). In the comparison, the saturation pressures of R123 and R134a are 158 and 1100 kPa, respectively, and the vapor quality is 0.2. The initial liquid film thickness ratio and the liquid film thickness decrement ratio of R134a to R123 are 1.5 and 0.45 from the calculation, respectively. The calculation results indicate that the liquid film thickness is thicker in the flow boiling of R134a than R123 because the initial film thickness is thicker and the decrement is smaller in the flow boiling of R134a. In addition, the thermal conductivities of liquid phase are similar between R123 and R134a at each saturation pressure. The heat transfer coefficients, therefore, must be smaller in the flow boiling of R134a, if the identical heat transfer mechanism with R123 is applied to the case of R134a. Experimental results, however, show that the heat transfer coefficients of R134a are much higher than those of R123. It definitely implies that another physical mechanism different from that of R123 plays an important role in the flow boiling of R134a.

The experimental results of R134a show that the heat transfer characteristics are similar to those of nucleate boiling at low and intermediate vapor quality while the experimental data of R123 do not. The examination of the wall superheat ($\Delta T_{SAT} = T_{wi} - T_{SAT}$) requirement for nucleate boiling, therefore, can help us to identify the dominant heat transfer mechanism of R134a and the criterion between the heat transfer mechanisms found in the boiling experiments of R123 and R134a. Davis and Anderson (1966) analytically derived the wall superheat requirement for imposed heat flux with the approximation that a temperature gradient away from the wall is linear. When heat flux and pressure are so low that the wall superheat requirement is limited by maximum active cavity size, the wall superheat requirement is calculated as follows; present experimental conditions for R123 and R134a correspond to this case.

$$\Delta T_{SAT} = \frac{R \cdot T_{SAT}^2 \cdot \ln(1+\zeta)/(i_{fg} \cdot M)}{1 - R \cdot T_{SAT} \cdot \ln(1+\zeta)/(i_{fg} \cdot M)} + \frac{q'' \cdot r_a}{k_L}, \quad \zeta = \frac{2 \cdot \sigma}{P_L \cdot r_a} \tag{21}$$

where R is the universal gas constant, M is molecular weight, r_a is maximum active cavity size and P_L is the imposed liquid pressure corresponding to saturation temperature T_{SAT}, namely saturation pressure in flow boiling. This means that nucleate boiling on the surface is only maintained in flow boiling when the wall superheat is larger than that given by Eq. (21) at the imposed heat flux. If the two-phase forced convective heat transfer coefficient becomes so high with increasing vapor quality that the wall superheat is less than that determined by Eq. (21), nucleate boiling is suppressed and no more takes place. If the two-phase forced convective heat transfer coefficient (h_{TP}) is known at the specified vapor quality, the minimum heat flux for nucleate boiling at that point can be calculated by substituting q''/h_{TP} for ΔT_{SAT} in Eq. (21). The minimum heat fluxes for R123 and R134a are calculated in present experimental conditions. The flow boiling heat transfer of R123 in present experimental conditions is dominated by the two-phase forced convection, specifically the evaporative heat transfer of thin liquid films around elongated bubbles. The two-phase forced convective heat transfer coefficients of R123 necessary for the calculation, therefore, are obtained from the heat transfer coefficients measured in the experiment. In addition, the two-phase forced convective heat transfer coefficients of R134a are approximated from those of R123 with the initial liquid film thickness ratio of R134a to R123 calculated from Eq. (11). The maximum active cavity size of 0.5 μm which is suggested for refrigerants by Collier and Thome (1994) is used in the calculation. As the calculation result, the minimum heat flux for nucleate boiling at the vapor quality of 0.2 ranges from 33.0 to 53.6 kW/m^2 for R123 and from 2.4 to 3.8 kW/m^2 for R134a when the saturation pressures of R123 and R134a are 158 and 1100 kPa, respectively. The calculation results indicate that the flow boiling of R123 has the suppression of nucleate boiling at even low vapor quality like 0.2 for the present heat flux condition (10–20 kW/m^2), while nucleate boiling is maintained in the flow boiling case of R134a. One reason for this suppression is the high wall superheat requirement of R123 for nucleate boiling. The larger surface tension and the lower saturation pressure of R123 in the present experimental condition make higher wall superheat requirement for identical heat flux than R134a. In macro-channels, this nucleate boiling suppression, however, does not often occur at low vapor quality like 0.2 except for the very low heat flux condition although the wall superheat requirement is high. It is because the heat transfer coefficient in the absence of nucleate boiling at low vapor quality is low enough to satisfy the wall superheat requirement. The wall superheat requirement, on the other hand, is more critical in micro-channels. The heat transfer coefficient generally increases with the reduction of channel diameter for identical mass velocity. Especially, the two-phase flow in micro-channels has very high heat transfer coefficients at even low vapor quality because of its dominant flow pattern, namely elongated bubble flow where the heat is transferred through the very thin liquid film formed around elongated bubbles. It makes the suppression take place at low vapor quality for the fluid like R123 which needs high wall superheat for nucleate boiling. If nucleate boiling is suppressed at low vapor quality like the case of R123, heat transfer is dominated by the evaporation of thin liquid films around elongated bubbles. In the contrary case such as R134a, nucleate boiling is maintained and it operates as the dominant heat transfer mechanism until its suppression at high vapor quality. The consideration of the wall superheat requirement or minimum heat flux for nucleate boiling, therefore, is an important factor in micro-channel flow boiling because the heat transfer trend and mechanism greatly depend on it.

Fig. 11 shows the comparison of heat transfer coefficients measured for R134a with those predicted by the Cooper (1984) correlation which is recommended for nucleate boiling of refrigerants and used as the contribution term of nucleate boiling in the flow boiling of macro-channels. The correlation is as follows.

$$h = 55 \cdot P_r^{0.12} (-0.4343 \cdot \ln P_r)^{-0.55} M^{-0.5} q''^{0.67} \tag{22}$$

where P_r is reduced pressure, the ratio of pressure to its critical pressure, M is molecular weight and q'' is heat flux. The correlation covers the reduced pressures from 0.001 to 0.9 and the molecular weights from 2 to 200 kg/kmol. The comparison is made for the

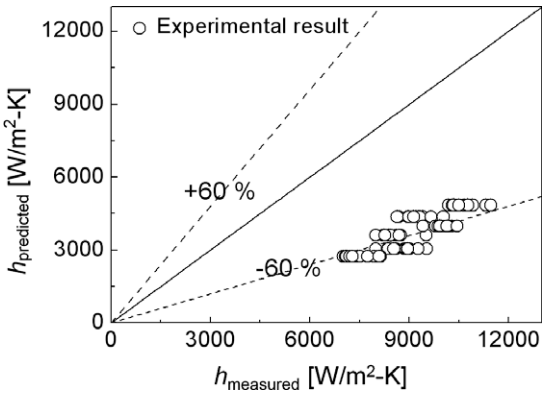

Fig. 11. Comparison of heat transfer coefficients measured for R134a with those predicted by the Cooper (1984) correlation.

vapor quality of 0.6 and less where the contribution of nucleate boiling is considered dominant. Fig. 11 indicates that the Cooper (1984) correlation considerably underestimates experimental results. Owhaib et al. (2004) reported that the heat transfer coefficient was in inverse proportion to channel diameter in their flow boiling experiment for micro-channels where the heat transfer trends of nucleate boiling were also dominant. However, they did not compare their results with existing heat transfer correlations. In addition, Bao et al. (2000) and Yun et al. (2005) reported that the Cooper (1984) correlation made a good prediction about their experiments where the hydraulic diameters of channels were approximately 6–10 times larger than that of the present experiment. Hence, the high heat transfer coefficient in the nucleate boiling dominant region of the present experiment beyond that of macro-channels predicted by Cooper (1984) correlation is considered as the result of its extremely small channel diameter. It also indicates that the enhancement of nucleate boiling related to the reduction of channel diameter is the feature of the micro-channel flow boiling which is distinguished from that of macro-channels. This enhancement may be explained by the following. The heat in nucleate boiling is generally transferred by three mechanisms: bubble agitation induced by growing and departing bubbles, thermal boundary layer stripping by departing bubbles and evaporation of the micro-layer trapped beneath bubbles. As channel diameter decreases and approaches to the detachment diameter of bubbles, bubbles grow and get detached in more narrow space. The narrow space results in more interference among bubbles or with the channel wall and increases the effects of bubble agitation and thermal boundary layer stripping. Growing bubbles may be also squeezed by the channel wall or other neighboring bubbles. It results in the larger surface area or the thinner thickness of the micro-layer and improves the effect of evaporation. The reduction of channel diameter, therefore, contributes to the enhancement of nucleate boiling heat transfer in the flow boiling of micro-channels. Following the nucleate boiling dominant region, a two-phase forced convection region is observed at the high vapor quality ($x > 0.6$) of experimental results. In the two-phase forced convection region, the effects of mass velocity and vapor quality are dominant but the effects of heat flux and saturation pressure are small. This forced convection region results from the suppression of nucleate boiling which also occurs in the flow boiling of macro-channels because the two-phase heat transfer coefficient in the absence of nucleation increases in proportion to vapor quality.

When the early suppression of nucleate boiling does not occur like the experiment of R134a, the flow boiling heat transfer mechanism of micro-channels is similar to that of macro-channels in that it is composed of nucleate boiling and two-phase forced convection. It, however, is different from that of macro-channels in that the enhancement of nucleate boiling related to the reduction of channel diameter exists, and the range of the two-phase forced convection region is relatively narrow and is limited to high vapor quality.

4.4. Comparison with recent heat transfer correlations for micro-channels

Present experimental data are compared with three heat transfer correlations recently suggested by Bertsch et al. (2009), Lee and Mudawar (2005) and Kandlikar and Balasubramanian (2004) for the flow boiling heat transfer of micro-channels. The detailed equations for each correlation are given in Table 4. The following is the brief description for each correlation.

Bertsch et al. (2009) developed their correlation based on the database of 3899 data points from 14 studies in the literature. The database covered 12 different wetting and non-wetting fluids, hydraulic diameters from 0.16 to 2.92 mm, confinement numbers from 0.3 to 4.0, mass velocities from 20 to 3000 kg/m^2 s, heat fluxes from 0.4 to 115 W/cm^2 and saturation temperatures from −194 to 97 °C. Lee and Mudawar (2005) suggested the flow boiling heat transfer correlation for micro-channels from their experimental data for R134a and micro-channel water data measured by Qu and Mudawar (2003). The rectangular channel of 231 × 713 μm was used as a test channel in both experiments. The experimental conditions were mass velocities from 127 to 654 kg/m^2 s, heat fluxes from 159 to 938 kW/m^2 and inlet pressures from 1.44 to 6.60 bar for R134a; mass velocities from 135 to 402 kg/m^2 s, inlet temperatures of 30 and 60 °C, and outlet pressure of 1.17 bar for water. In Table 4, the single phase heat transfer coefficients of liquid and vapor, $h_{sp,L}$ and $h_{sp,V}$, are modified from the original equations which the authors presented to be applicable to our circular channel geometry with uniform circumferential heating. Kandlikar and Balasubramanian (2004) extended the Kandlikar (1990) correlation for macro-channels to the region of mini- and micro-channels with some modification. They compared their correlation with experimental data for micro-channels, and reported a good agreement between them. The Nusselt number (Nu) for laminar flow at a uniform heat flux condition, specifically 4.36, is used in the comparison with present experimental data.

Fig. 12(a)–(c) compares the heat transfer coefficients predicted by each correlation with those measured in the present experiment. In addition, Table 5 indicates the mean absolute error of each correlation. The mean absolute error is defined as

$$\mathrm{MAE} = \frac{1}{N}\cdot\sum_{N}\left[\frac{|h_{pred} - h_{exp}|}{h_{exp}} \times 100\right] \tag{23}$$

where h_{exp} and h_{pred} are the heat transfer coefficients measured in the present experiment and predicted by the correlation respectively, and N is the number of experimental data. Fig. 12 and Table 5 show that all three correlations make poor predictions of present experimental data. The correlations were also compared with various experimental data sets in the literature, Bertsch et al. (2009) and Lee et al. (2007) where they made good predictions of some experimental data sets but poor predictions of others like present experimental data. The comparisons in the present study and the literature indicate that these correlations predict a portion of total experimental data with allowable error and, therefore, they achieve only partial success. It suggests the need of the systematically subdivided heat transfer correlation based on the heat transfer mechanism for more accurate prediction.

5. Conclusions

Flow boiling heat transfer in a single circular micro-channel of 0.19 mm has been experimentally studied with R123 and R134a

Table 4
Previous flow boiling heat transfer correlations for micro-channels.

Author	Correlation
Bertsch et al. (2009)	$h = h_{NB} \cdot (1-x) + h_{CB} \cdot \{1 + 80 \cdot (x^2 - x^6) \cdot e^{-0.6 \cdot Co}\}$
	$h_{NB} = 55 \cdot P_r^{0.12} (-0.4343 \cdot \ln P_r)^{-0.55} M^{-0.5} q''^{0.67}$
	$h_{CB} = h_{conv,L} \cdot (1-x) + h_{conv,V} \cdot x$
	$h_{conv,L} = \left(3.66 + \frac{0.0668 \cdot D_h / L \cdot Re_L \cdot Pr_L}{1 + 0.04 \cdot [D_h / L \cdot Re_L \cdot Pr_L]^{2/3}}\right) \cdot \frac{k_L}{D_h}$
	$h_{conv,V} = \left(3.66 + \frac{0.0668 \cdot D_h / L \cdot Re_V \cdot Pr_V}{1 + 0.04 \cdot [D_h / L \cdot Re_V \cdot Pr_V]^{2/3}}\right) \cdot \frac{k_V}{D_h}$
	$Co = \left[\frac{\sigma}{g(\rho_L - \rho_V) D_h^2}\right]^{1/2}$
	$Re_L = \frac{G \cdot D_h}{\mu_L}$, $Re_V = \frac{G \cdot D_h}{\mu_V}$, $Pr_L = \frac{c_{p,L} \cdot \mu_L}{k_L}$, $Pr_V = \frac{c_{p,V} \cdot \mu_V}{k_V}$
Lee and Mudawar (2005)	$h = 3.856 \cdot X^{0.267} \cdot h_{sp,L} \quad (x = 0 - 0.05)$
	$h = 436.48 \cdot Bo^{0.522} \cdot We_L^{0.351} \cdot X^{0.665} \cdot h_{sp,L} \quad (x = 0.05 - 0.55)$
	$h = \max\{(108.6 \cdot X^{1.665} \cdot h_{sp,V}), h_{sp,V}\} \quad (x = 0.55 - 1.0)$
	$h_{sp,L} = 4.36 \cdot \frac{k_L}{D_h}$
	$h_{sp,V} = 4.36 \cdot \frac{k_V}{D_h}$ for laminar vapor flow,
	$h_{sp,V} = 0.023 \cdot Re_V^{0.8} \cdot Pr_V^{0.4} \cdot \frac{k_V}{D_h}$ for turbulent vapor flow
	$X = \left(\frac{\mu_L}{\mu_V}\right)^{0.5} \cdot \left(\frac{\rho_V}{\rho_L}\right)^{0.5} \cdot \left(\frac{1-x}{x}\right)^{0.5}$ for laminar liquid – laminar vapor
	$X = \frac{13.315}{Re_V^{3/8}} \cdot \left(\frac{\mu_L}{\mu_V}\right)^{0.5} \cdot \left(\frac{\rho_V}{\rho_L}\right)^{0.5} \cdot \left(\frac{1-x}{x}\right)^{0.5}$ for laminar liquid – turbulent vapor
	$Bo = \frac{q''}{G \cdot i_{fg}}$, $We_L = \frac{G^2 \cdot D_h}{\sigma \cdot \rho_L}$, $Re_V = \frac{G \cdot x \cdot D_h}{\mu_V}$, $Pr_V = \frac{c_{p,V} \cdot \mu_V}{k_V}$
Kandlikar and Balasubramanian (2004)	$h = \max(h_{NBD}, h_{CBD}) \quad (100 < Re_{LO} < 1600)$
	$h = h_{NBD} \quad (Re_{LO} \le 100)$
	$h_{NBD} = 0.6683 \cdot Co^{-0.2} \cdot (1-x)^{0.8} \cdot h_{LO} + 1058.0 \cdot Bo^{0.7} \cdot (1-x)^{0.8} \cdot F_{Fl} \cdot h_{LO}$
	$h_{CBD} = 1.136 \cdot Co^{-0.9} \cdot (1-x)^{0.8} \cdot h_{LO} + 667.2 \cdot Bo^{0.7} \cdot (1-x)^{0.8} \cdot F_{Fl} \cdot h_{LO}$
	$h_{LO} = \frac{Nu \cdot k_L}{D_h}$
	$Re_{LO} = \frac{G \cdot D_h}{\mu_L}$, $Co = \left(\frac{\rho_V}{\rho_L}\right)^{0.5} \cdot \left(\frac{1-x}{x}\right)^{0.8}$, $Bo = \frac{q''}{G \cdot i_{fg}}$
	$F_{Fl} = 1$ for a stainless steel tube regardless of fluid

for various experimental conditions: heat fluxes, mass velocities, vapor qualities and different saturation pressures. The test fluids of R123 and R134a have considerable differences of properties at ambient saturation temperature, such as saturation pressure, surface tension and liquid viscosity. They affect heat transfer trends and mechanisms in the flow boiling of micro-channels. The following conclusions are derived from the experimental results and the analysis for them.

(a) The heat transfer trends between R123 and R134a are distinctive. The flow boiling heat transfer of R123 shows that the heat transfer coefficients depend on mass velocity, heat flux and vapor quality. The saturation pressure effect depends on the experimental conditions: mass velocity and heat flux. Especially, the effects of mass velocity and heat flux are increased as saturation pressure decreases. On the contrary, the heat transfer trends of R134a are similar to those of macro-channels, not identical though. The heat transfer coefficients are strongly dependent on heat flux and saturation pressure at low and intermediate vapor quality, but the effects of mass velocity and vapor quality are insignificant. At high vapor quality, the mass velocity effect is dominant while the effects of heat flux and saturation pressure are small.
(b) The heat transfer characteristics of R123 are well described by the behavior of liquid film thickness around elongated bubbles which is related to the evaporative heat transfer. It

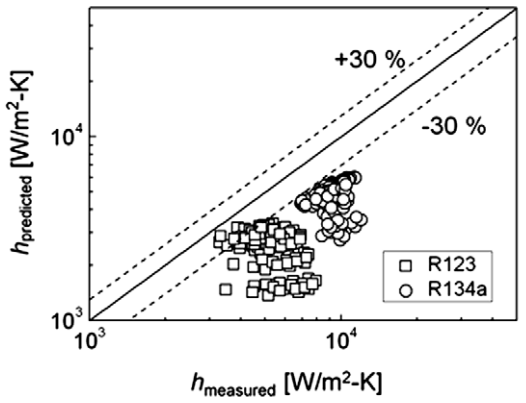

(a) Correlation by Bertsch et al. (2009)

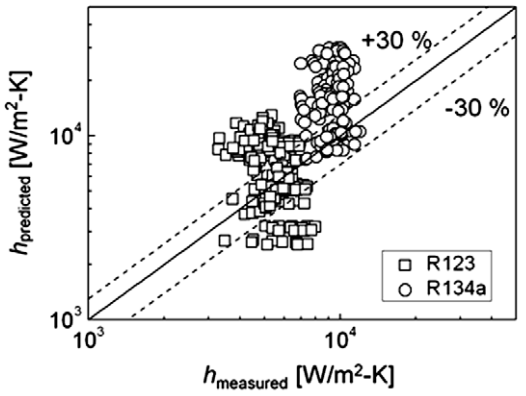

(b) Correlation by Lee and Mudawar (2005)

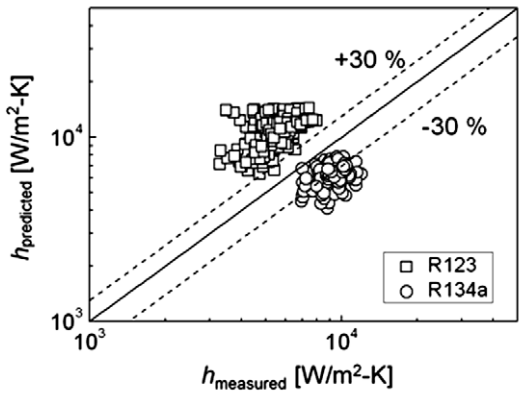

(c) Correlation by Kandlikar and Balasubramanian (2004)

Fig. 12. Comparison of previous heat transfer correlations with present experimental data.

suggests that the flow boiling heat transfer of R123 is dominated by the evaporation of thin liquid films around elongated bubbles.

Table 5
Mean absolute error of each correlation.

Correlation	MAE for R123 data (%)	MAE for R134a data (%)	MAE for total data (%)
Bertsch et al. (2009)	51.6	48.7	50.3
Lee and Mudawar (2005)	56.1	81.1	67.6
Kandlikar and Balasubramanian (2004)	95.4	31.1	65.9

(c) The wall superheat requirement for nucleate boiling is very critical in micro-channels because the two-phase flow in micro-channels has very high convective heat transfer coefficients at even low vapor quality due to its dominant flow pattern of elongated bubble flow and consequently the early suppression of nucleate boiling can easily occur. Whether the early suppression of nucleate boiling occurs or not determines the heat transfer trends and mechanisms in the flow boiling of micro-channels. If the wall superheat requirement is not satisfied and the nucleate boiling is suppressed at low vapor quality, heat transfer is dominated by the evaporation of thin liquid films around elongated bubbles like R123. In the contrary case, nucleate boiling is maintained and it operates as the dominant heat transfer mechanism until its suppression at high vapor quality. This corresponds to the case of R134a.

(d) In the absence of the early suppression of nucleate boiling, the heat transfer mechanism is similar to that of macro-channels which is composed of nucleate boiling and two-phase forced convection. It, however, is distinguished from macro-channels in that the enhancement of nucleate boiling related to the small channel size exists, and the range of the two-phase forced convection region is relatively narrow and limited to high vapor quality.

(e) Three recent heat transfer correlations by Bertsch et al. (2009), Lee and Mudawar (2005) and Kandlikar and Balasubramanian (2004) are compared with present experimental data. None of them give satisfactory predictions of the present experimental data. These correlations achieve only partial success of predicting a portion of experimental data with allowable error, which is also supported by the related literature. A systematically subdivided heat transfer correlation based on the physical mechanism is necessary for more accurate prediction.

Acknowledgements

This work was supported by the Korea Science and Engineering Foundation (KOSEF) grant funded by the Korea government (MEST) (No. R0A-2007-000-20062-0).

Appendix A. Correlations for bubble departure diameter in nucleate pool boiling

Borishanskiy et al. (1981) presented the correlation for bubble departure diameter as follows.

$$d_h = 5 \times 10^5 \left(\frac{P}{P_c}\right)^{-0.46} \left(\frac{K \cdot T_c}{P_c \cdot M}\right)^{1/3} \tag{A1}$$

where P is pressure, P_c is critical pressure, K is the Boltzmann constant (1.38×10^{-23} J/K), T_c is critical temperature and M is molecular weight. Kutateladze and Gogonin (1979), on the other hand, proposed the correlation as

$$d_h = 0.25 \cdot (1 + 10^5 \cdot K_1)^{1/2} \cdot \sqrt{\frac{\sigma}{g(\rho_L - \rho_V)}} \quad \text{for } K_1 < 0.06 \tag{A2}$$

where σ is surface tension, g is the gravitational acceleration, ρ_L and ρ_V are the densities of liquid and vapor phases, respectively, and K_1 is the dimensionless parameter defined as

$$K_1 = \left(\frac{\mathrm{Ja}}{\mathrm{Pr_L}}\right)^2 \cdot \left\{\left[\frac{g \cdot \rho_L(\rho_L - \rho_V)}{\mu_L^2}\right] \cdot \left[\frac{\sigma}{g(\rho_L - \rho_V)}\right]^{3/2}\right\}^{-1} \quad \text{(A3)}$$

$$\mathrm{Ja} = \frac{\rho_L \cdot c_{P,L} \cdot \Delta T_{SAT}}{\rho_V \cdot i_{fg}} \quad \text{(A4)}$$

$$\mathrm{Pr_L} = \frac{c_{P,L} \cdot \mu_L}{k_L} \quad \text{(A5)}$$

where Ja is the Jacob number, $\mathrm{Pr_L}$ is the Prandtl number of liquid phase, μ_L is the viscosity of liquid phase, i_{fg} is the enthalpy of vaporization, $c_{p,L}$ is the specific heat of liquid phase at constant pressure, ΔT_{SAT} is the wall superheat of the difference between wall temperature and saturation temperature ($T_{wi} - T_{SAT}$) and k_L is the thermal conductivity of liquid phase. Jensen and Memmel (1986) modified the Kutateladze and Gogonin (1979) correlation on the basis of available bubble departure diameter data.

$$d_h = 0.19 \cdot (1.8 + 10^5 \cdot K_1)^{2/3} \cdot \sqrt{\frac{\sigma}{g(\rho_L - \rho_V)}} \quad \text{(A6)}$$

where the dimensionless parameter, K_1 is identical with that of the Kutateladze and Gogonin (1979) correlation.

References

Aussillous, P., Quéré, D., 2000. Quick deposition of a fluid on the wall of a tube. Phys. Fluids 12, 2367–2371.

Bao, Z.Y., Fletcher, D.F., Haynes, B.S., 2000. Flow boiling heat transfer of Freon R11 and HCFC123 in narrow passages. Int. J. Heat Mass Transfer 43, 3347–3358.

Bertsch, S.S., Groll, E.A., Garimella, S.V., 2009. A composite heat transfer correlation for saturated flow boiling in small channels. Int. J. Heat Mass Transfer 52, 2110–2118.

Borishanskiy, V.M., Danilova, G.N., Gotovskiy, M.A., Borishanskiy, A.V., Danilova, G.P., Kupriyanova, A.V., 1981. Correlation of data on heat transfer in, and elementary characteristics of the nucleate boiling mechanism. Heat Trans. – Sov. Res. 13 (1), 100–116.

Chisholm, D., 1983. Two-phase Flow in Pipelines and Heat Exchangers. Pitman Press, Bath, UK.

Collier, J.G., Thome, J.R., 1994. Convective Boiling and Condensation. Clarendon Press, Oxford.

Cooper, M.G., 1984. Heat flow rates in saturated nucleate pool boiling – a wide-ranging examination using reduced properties. Adv. Heat Transfer 16, 157–239.

Davis, E.J., Anderson, G.H., 1966. The incipience of nucleate boiling in forced convection flow. AIChE J. 12, 774–780.

Dupont, V., Thome, J.R., 2004. Evaporation in microchannels: influence of the channel diameter on heat transfer. In: Proc. of the 2nd Int. Conf. on Microchannels and Minichannels, pp. 461–468.

Dupont, V., Thome, J.R., Jacobi, A.M., 2004. Heat transfer model for evaporation in microchannels. Part II: Comparison with the database. Int. J. Heat Mass Transfer 47, 3387–3401.

Jacobi, A.M., Thome, J.R., 2002. Heat transfer model for evaporation of elongated bubble flows in microchannels. J. Heat Transfer 124, 1131–1136.

Jensen, J. and Memmel, G. J., 1986. Evaluation of bubble departure diameter correlations. In: Proc. of the 8th Int. Heat Transfer Conf., pp. 1907–1912.

Kandlikar, S.G., 1990. A general correlation for two-phase flow boiling heat transfer coefficient inside horizontal and vertical tubes. J. Heat Transfer 102, 219–228.

Kandlikar, S.G., 2002. Two-phase flow patterns, pressure drop, and heat transfer during boiling in minichannel flow passages of compact evaporators. Heat Transfer Eng. 23 (1), 5–23.

Kandlikar, S.G., Balasubramanian, P., 2004. An extension of the flow boiling correlation to transition, laminar, and deep laminar flows in minichannels and microchannels. Heat Transfer Eng. 25 (3), 86–93.

Kandlikar, S.G., Grande, W.J., 2003. Evolution of microchannel flow passages-thermohydraulic performance and fabrication technology. Heat Transfer Eng. 24 (1), 3–17.

Kawahara, A., Chung, P.M.-Y., Kawaji, M., 2002. Investigation of two-phase flow pattern, void fraction and pressure drop in a microchannel. Int. J. Multiphase Flow 28, 1411–1435.

Kays, W.M., Crawford, M.E., 1993. Convective Heat and Mass Transfer. McGraw-Hill, New York.

Kew, P.A., Cornwell, K., 1997. Correlations for the prediction of boiling heat transfer in small-diameter channels. Appl. Therm. Eng. 17, 705–715.

Kolb, G., Schürer, J., Tiemann, D., Wichert, M., Zapf, R., Hessel, V., Löwe, H., 2007. Fuel processing in integrated micro-structured heat-exchanger reactors. J. Power Sources 171, 198–204.

Kutateladze, S.S., Gogonin, I.I., 1979. Growth rate and detachment diameter of a vapor bubble in free convection boiling of a saturated liquid. High Temp. 17, 667–671.

Lee, H.J., Liu, D., Yao, S.C., Alyousef, Y., 2007. Generalized two-phase pressure drop and heat transfer correlations in evaporative micro/mini-channels. In: Proc. of the 2007 ASME–JSME Therm. Eng. Summer Heat Transfer Conf., #32157.

Lee, J., Mudawar, I., 2005. Two-phase flow in high-heat-flux micro-channel heat sink for refrigeration cooling applications: part II – heat transfer characteristics. Int. J. Heat Mass Transfer 48, 941–955.

Lie, Y.M., Lin, T.F., 2005. Saturated flow boiling heat transfer and associated bubble characteristics of R-134a in a narrow annular duct. Int. J. Heat Mass Transfer 48, 5602–5615.

Marquardt, E.D., Radebaugh, R., Dobak, J., 1998. A cryogenic catheter for treating heart arrhythmia. Adv. Cryog. Eng. 43, 903–910.

Moriyama, K., Inoue, A., 1996. Thickness of the liquid film formed by a growing bubble in a narrow gap between two horizontal plates. J. Heat Transfer 118, 132–139.

Munkejord, S.T., Mæhlum, H.S., Zakeri, G.R., Nekså, P., Pettersen, J., 2002. Micro technology in heat pumping systems. Int. J. Refrig. 25, 471–478.

Ohta, H., Inoue, K., Shimada, Y., 2006. Experimental study on flow boiling heat transfer in an extremely small tube. In: Proc. of the 4th Int. Conf. on Nanochannels, Microchannels and Minichannels, #96177.

Owhaib, W., Martín-Callizo, C., Palm, B., 2004. Evaporative heat transfer in vertical circular microchannels. Appl. Therm. Eng. 24, 1241–1253.

Qu, W., Mudawar, I., 2003. Flow boiling heat transfer in two-phase micro-channel heat sinks – I. Experimental investigation and assessment of correlation methods. Int. J. Heat Mass Transfer 46, 2755–2771.

Ribatski, G., Wojtan, L., Thome, J.R., 2006. An analysis of experimental data and prediction methods for two-phase frictional pressure drop and flow boiling heat transfer in micro-scale channels. Exp. Therm. Fluid Sci. 31, 1–19.

Taylor, B.N., Kuyatt, C.E., 1994. Guidelines for evaluating and expressing the uncertainty of NIST measurement results. NIST Technical Note, p. 1297.

Thome, J.R., 2004. Boiling in microchannels: a review of experiment and theory. Int. J. Heat Fluid Flow 25, 128–139.

Thome, J.R., Dupont, V., Jacobi, A.M., 2004. Heat transfer model for evaporation in microchannels. Part I: Presentation of the model. Int. J. Heat Mass Transfer 47, 3375–3385.

Yan, Y.Y., Lin, T.F., 1998. Evaporation heat transfer and pressure drop of refrigerant R-134a in a small pipe. Int. J. Heat Mass Transfer 41, 4183–4194.

Yun, R., Kim, Y., Kim, M.S., 2005. Convective boiling heat transfer characteristics of CO_2 in microchannels. Int. J. Heat Mass Transfer 48, 235–242.